JACS
JOURNAL OF THE AMERICAN CHEMICAL SOCIETY

Article

pubs.acs.org/JACS

Carbon Dioxide in a Supported Ionic Liquid Membrane: Structural and Rotational Dynamics Measured with 2D IR and Pump–Probe Experiments

Jae Yoon Shin, Steven A. Yamada, and Michael D. Fayer*

Department of Chemistry, Stanford University, Stanford, California 94305, United States

Supporting Information

ABSTRACT: Supported ionic liquid membranes (SILMs) are porous membranes impregnated with ionic liquids (ILs) and used as advanced carbon capture materials. Here, two-dimensional infrared (2D IR) and IR polarization selective pump–probe (PSPP) spectroscopies were used to investigate CO_2 reorientation and spectral diffusion dynamics in SILMs. The SILM contained 1-ethyl-3-methylimidazolium bis-(trifluoromethylsulfonly)imide in the poly(ether sulfone) membrane with average pore size of ∼350 nm. Two ensembles of CO_2 were observed in the SILM, one in the IL phase in the membrane pores and the other in the supporting membrane polymer. CO_2 in the polymer displayed a red-shifted IR absorption spectrum and a shorter vibrational lifetime of the asymmetric stretch mode compared to the IL phase. Despite the relatively large pore sizes, the complete orientational randomization of CO_2 and structural fluctuations of the IL (spectral diffusion) in the pores are slower than in the bulk IL by ∼2-fold. The implication is that the IL structural change induced by the polymer interface can propagate out from the interface more than a hundred nanometers, influencing the dynamics. The dynamics in the polymer are even slower. This study demonstrates that there are significant differences in the dynamics of ILs in SILMs on a molecular level compared to the bulk IL, and the study of dynamics in SILMs can provide important information for the design of SILMs for CO_2 capture.

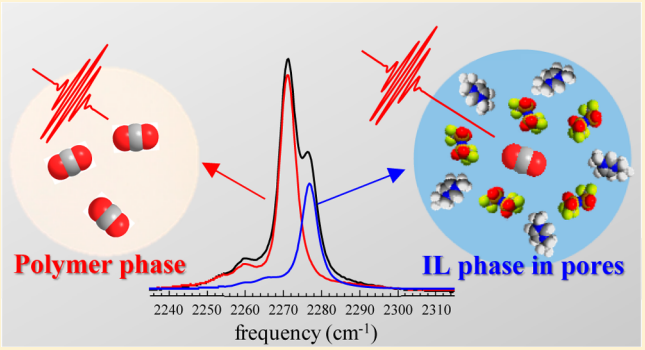

1. INTRODUCTION

The rise in the atmospheric concentration of the major anthropogenic greenhouse gas, carbon dioxide, has been accelerated since the industrial revolution, resulting in the onset of global warming and climate change that will cause severe effects on humanity.[1−3] Thus, reducing the current level of CO_2 emission into the atmosphere is important to global society, and carbon capture and storage (CCS) from stationary sources is an important goal.[4,5] In the CCS process, CO_2 is captured before it enters to the atmosphere. Currently, the capture process is expensive, inhibiting the practical application of CCS. In many approaches, regenerating the capture material after CO_2 separation requires substantial energy.[5] Therefore, developing efficient methods and materials for CO_2 capture is the key to the accomplishments of CCS.

Ionic liquids (ILs) are molten salts, consisting of complex cations and anions, that have melting points below 100 °C.[6] ILs that remain as liquids at room temperature are called RTILs. RTILs have been of great interest as one of promising media for carbon capture because they have negligible volatility,[7] low flammability,[8] high thermal stability,[9] and more importantly, high tunability of their physical and chemical properties.[6,10] Degradations and loss of the capture medium, which are major flaws of using organic solvents in carbon capture, can be essentially eliminated by using RTILs.[11−13]

Supported ionic liquid membranes (SILMs) are advanced materials for carbon capture and separation. The SILMs are, in general, based on organic or inorganic porous membranes whose pores are filled with RTILs.[14−17] SILMs are highly cost and energy efficient because they have a large surface area for CO_2 capture and diffusion of CO_2 through the RTIL in the pores provides an avenue for capture of the CO_2 without the need for a solvent regeneration process.[14−17] Therefore, various types of SILMs have been developed and examined to optimize their permeability and selectivity for applications.[17] In addition, there has been extensive studies on nanoconfined ILs in various porous materials to understand physicochemical properties and dynamics of ILs on a molecular level, using different experimental techniques.[18−23] Yet, ultrafast spectroscopic studies of these systems are rare although the fundamental time scales of molecular dynamics are usually on picosecond scale.

Recently, ultrafast time-resolved IR spectroscopies were employed to investigate the dynamics of CO_2 in bulk RTILs.[24−26] These bulk IL experiments were conducted as a function of alkyl chain length on 1-ethyl-3-methylimidazolium bis(trifluoromethylsulfonyl)imide (EmimNTf$_2$) and with 4, 6,

Received: June 3, 2017
Published: July 19, 2017

© 2017 American Chemical Society

DOI: 10.1021/jacs.7b05759
J. Am. Chem. Soc. 2017, 139, 11222−11232

and 10 carbon chain lengths on the imidizolium. Prior to the study of CO_2 in these bulk RTILs, the small anion, $SeCN^-$, was used as the vibrational probe to investigate the same series of bulk RTILs.[27,28] In the first study of the dynamics of RTILs in SLIMs, $SeCN^-$ in $EmimNTf_2$ was used as the vibrational probe. The results of these studies using ultrafast two-dimensional infrared (2D IR) spectroscopy and IR polarization selective pump−probe (PSPP) experiments demonstrated that the RTIL dynamics in the SILMs was substantially slower than in the bulk.[29] Therefore, the dynamical properties of ILs in SILMs cannot be obtained from studies of the bulk liquid.[29] Thus, measurements of molecular interactions and dynamics in SILMs are important for developing an understanding of SILMs for technological applications.

In this study, the orientational and structural dynamics were investigated using PSPP and 2D IR spectroscopies applied to SILMs containing $^{13}CO_2$, which were prepared with $EmimNTf_2$ and poly(ether sulfone) (PES) membranes. Although the same SILM was previously examined with $SeCN^-$ vibrational probe due to the ease of sample preparation,[29] CO_2 is the relevant solute for investigating SILMs for CO_2 capture. Unlike $SeCN^-$, $^{13}CO_2$ in the SILM samples existed in two distinct ensembles, that is, in the IL and in the polymer itself. Two well resolved CO_2 asymmetric stretch bands were observed in the Fourier transform infrared (FT-IR) spectrum of the SILM sample. The blue-shifted (higher frequency) band is the same as observed in the bulk RTIL. The CO_2 observed in the additional (lower frequency) band in the membrane polymer exhibits very different behavior from the ensemble in the IL phase. The dynamics of the CO_2 ensemble in the polymer are much slower than they are in the IL in the SILM, which in turn are slower than the dynamics in the bulk IL.

The PES membrane used in this study has very large pores, with the average pore size of ∼350 nm.[29] The fact that both the CO_2 and $SeCN^-$ vibrational probes report on substantial slowing of the RTIL dynamics in such large pores is remarkable. For example, water in nanoscopic confinement in systems, like AOT reverse micelles, has bulk-like water behavior away from the interface once the diameter is greater than ∼5 nm.[30,31] Moreover, pulsed field gradient NMR study found that the diffusivities of CO_2 and IL decrease under condition of nanoconfinement in KIT-6 silica that has pore size of 8.5 nm, compared to the bulk condition.[19] The results presented here show that pore interface in SILMs produces long-range IL structuring that is different from the bulk IL structure. The change in IL structure in the pores and the slowing of the observed dynamics suggests that CO_2 translational diffusion will also be slowed. The translational diffusion coefficient of CO_2 in the pores, which is directly connected to the SILM's performance, was estimated using the complete orientational relaxation time measured by PSPP and the Stokes−Einstein (SE) equation.[32,33]

2. EXPERIMENTAL PROCEDURES

2.1. Sample Preparation. $EmimNTf_2$ was purchased from Iolitec and stored in a nitrogen glovebox after drying under vacuum (∼100 mTorr) at ∼65 °C. Isotopically labeled $^{13}CO_2$ (<99% isotopic purity) and poly(ether sulfone) membrane (Supor 200), abbreviated as PES200, were purchased from Icon Isotopes and Pall corporation, respectively. To prepare the SILM sample with $^{13}CO_2$, a piece of PES200 was soaked in $EmimNTf_2$ overnight. After the wet PES200 was wiped with lens tissues to remove excess $EmimNTf_2$ on its surface, it was transferred to a vial that had a cap with rubber septum. The air inside the vial was pumped out for 20 min and then, $^{13}CO_2$ gas was injected through a needle. The SILM was exposed to $^{13}CO_2$ for more than 20 min inside the vial so that it absorbs enough $^{13}CO_2$ for the experiments. On the basis of the extinction coefficient of asymmetric stretch band of CO_2 in water[34] and the absorbance of the sample, the concentration of $^{13}CO_2$ in the sample was calculated to be 400 ion pairs of $EmimNTf_2$ per a carbon dioxide molecule.

To determine how well the pores are filled with the IL, the PES200 membrane was weighed before and after the pore filling with surface wiping, and the amount of IL absorbed by the membrane was calculated. From the 25 mm diameter, 150-μm thickness, and 80% porosity of PES200, it was estimated that about 95% of the pores are filled by the SILM preparation. The prepared SILM sample was sandwiched between two one-inch CaF_2 windows with a 150-μm thick polytetrafluoroethylene (Teflon) ring spacer. The spacer thickness is comparable to that of PES200. To prevent the membrane from being in contact with the windows, 3.5-μm thick spacer, which was cut from thin film (Mylar TF-135, Premier Lab Supply) with a hole in the middle, was inserted between the SILM and window on both sides. This allows the SILM to be in a stand-alone mode, giving the same condition as in its practical application. In the FT-IR spectrum, there was no sign of free $^{13}CO_2$ gas that can diffuse out of the SILM into the 3.5-μm gap and would interfere with the signal in the laser experiments. Depending on the sample conditions, the 3.5-μm gap was often filled with a small amount of IL which came out from the SILM while the sample cell was assembled. However, the contributions of $^{13}CO_2$ in the IL trapped in this gap to the signal is negligible because the SILM is much thicker than the gap (2×3.5 μm vs 150 μm). The majority of the signal comes from $^{13}CO_2$ in the SILM. The sample cell was assembled under dry environment to avoid contamination with H_2O. Also, vacuum grease was applied to each layer of spacers for sealing the sample cell and avoiding escape of $^{13}CO_2$. The FT-IR spectra of the samples were collected using a Thermo Scientific Nicolet 6700 FT-IR spectrometer before and after the ultrafast IR experiments to confirm that there were no changes in the samples over time.

2.2. Time-resolved Ultrafast Infrared Experiments. The details of the experimental setup have been reported previously;[35] a brief description is presented here. A Ti:sapphire regenerative amplifier pumps a home-built optical parametric amplifier creating mid-IR pulses centered at 2277 cm^{-1} with ∼6 μJ pulse energy. An enclosure of the optical table was purged with H_2O and CO_2-scrubbed air to minimize atmospheric absorption. Because some CO_2 remained even with the purge, $^{13}CO_2$ that has its asymmetric stretch absorption shifted away from the $^{12}CO_2$ wavelength was used so that atmospheric $^{12}CO_2$ absorption did not affect the data.

The mid-IR beam was split into two beams, a stronger pump pulse and weaker probe pulse. The pump pulse was passed through an acousto-optic mid-IR Fourier-domain pulse-shaper. In the PSPP experiments, the pulse shaper chopped the pump pulse to obtain transient absorption signals, while in the 2D IR experiments the pulse shaper generated two excitation pulses, 1 and 2, and controlled the delay time (τ) between them. In addition, the pulse shaper controlled the phase of the pulses and was used to overcome light scattering that is the major difficulty in performing the laser experiments of membranes. A 4-shot phase cycling scheme[35] was used for the 2D IR experiments with perpendicular polarization configuration as well as for the PSPP. In the 2D IR measurements with parallel polarization configuration, in which the scattered light was a more serious problem, an 8-shot phase cycling and chopping scheme was utilized.[36] A mechanical delay stage in the probe pulse path controlled the time delay between the pump and probe pulses in the PSPP experiments or the time delay (waiting time, T_w) between the second excitation pulse 2 and the third excitation pulse 3 (probe pulse) in the 2D IR experiments. The pump and probe pulses were focused into the sample with a small crossing angle for both experiments. After passing through the sample, the probe pulse was directed into a spectrograph. The spectrograph disperses the probe pulse, which was then detected in the frequency-domain by a 32-pixel HgCdTe (MCT) IR array detector. The 2D IR signal is collinear with the third pulse (probe

DOI: 10.1021/jacs.7b05759
J. Am. Chem. Soc. 2017, 139, 11222−11232

pulse), which also acts as the local oscillator (LO) used for heterodyne detection of the signal.

In the PSPP measurements, the probe polarization was horizontal (in the plane of the optical table) and the pump polarization was at 45° with respect to the probe pulse. After the sample, a polarizer mounted in a computer controlled rotation stage alternately resolved the probe pulse at +45° (parallel to the pump) and −45° (perpendicular to the pump) relative to the incident polarization (horizontal). Since the response of the spectrograph grating is polarization-dependent, another horizontal polarizer was placed in front of the spectrometer's entrance slit to ensure that there is no bias in the detection of the polarizations. The collected probe signals parallel, $S_{\parallel}(t)$, and perpendicular, $S_{\perp}(t)$, to the pump were used to obtain the population relaxation $P(t)$ and the second Legendre polynomial orientational correlation function $C_2(t)$ using[37]

$$S_{\parallel}(t) = P(t)[1 + 0.8C_2(t)] \quad (1)$$

$$S_{\perp}(t) = P(t)[1 - 0.4C_2(t)] \quad (2)$$

From these, the population relaxation is given by

$$P(t) = \frac{1}{3}[S_{\parallel}(t) + 2S_{\perp}(t)] \quad (3)$$

The anisotropy, $r(t)$, is the transition dipole orientational correlation function (the second Legendre polynomial correlation function, $C_2(t) = \langle P_2(\hat{\mu}(t)\cdot\hat{\mu}(0))\rangle$), scaled by 0.4.

$$r(t) = \frac{S_{\parallel}(t) - S_{\perp}(t)}{S_{\parallel}(t) + 2S_{\perp}(t)} = 0.4C_2(t) \quad (4)$$

In the 2D IR vibrational echo experiments, three excitation pulses 1, 2, and 3 impinge on the sample with controllable time delays, τ (delay between 1 and 2 pulses) and T_w (delay between 2 and 3 pulses). In effect, pulses 1 and 2 label the initial frequencies of the $^{13}CO_2$ asymmetric stretch vibrational oscillators. After the system evolves during T_w, pulse 3 generates the vibrational echo signal, reading out the final frequencies of the vibrational oscillators. To carry out the polarization selective measurements, the polarization of both excitation pulses 1 and 2 was set to 0° and 90° relative to the probe polarization (horizontal) in the $\langle XXXX\rangle$ (parallel) and $\langle XXYY\rangle$ (perpendicular) configurations, respectively, using a polarizer and half-wave-plate. The resolving polarizer after the sample is fixed to horizontal and is not changed for either polarization configurations. The 2D IR spectrum consists of the ω_m (vertical) and ω_τ (horizontal) axes and requires two Fourier transforms to obtain the frequency domain spectrum. The first Fourier transform yields the ω_m axis experimentally by resolving the frequencies of echo/LO pulse via the spectrograph, that is, the time domain pulse is taken into the frequency domain. Scanning τ in the experiments produces an interferogram at each ω_m because the echo signal moves in phase relative to the fixed in time LO. The numerical Fourier transform of this interferogram for each ω_m gives the ω_τ axis of the 2D IR spectrum.

For each T_w, a 2D IR spectrum is collected by scanning τ, and the spectral diffusion is evaluated based on the 2D line shape analysis at each T_w. The T_w dependent frequency-frequency correlation function (FFCF) contains the dynamical information on interest. The center line slope (CLS) method[38,39] was employed to obtain the normalized FFCF (CLS(T_w)) from the 2D IR spectra. A plot of the CLS vs T_w is the normalized T_w-dependent portion of the FFCF. Given the CLS(T_w) and the linear absorption spectrum, the full FFCF including the homogeneous component can be determined.

3. RESULTS AND DISCUSSIONS

3.1. Linear IR Absorption Spectra. Figure 1A displays the IR absorption spectrum of $^{13}CO_2$ in the SILM (black) and $^{13}CO_2$ in the bulk IL (blue). $^{13}CO_2$ in the bulk IL has its asymmetric stretch at 2276 cm^{-1}. SeCN$^-$ in the PES200 SILM with the same IL previously showed a single peak as in its bulk sample.[29] However, $^{13}CO_2$ in the SILM has an additional

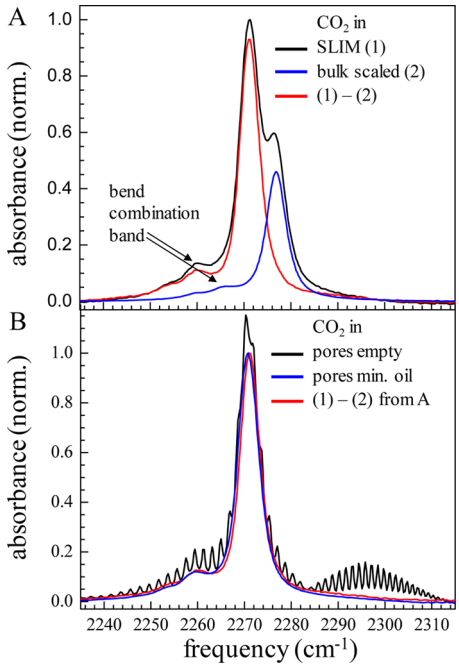

Figure 1. Background-subtracted FT-IR of $^{13}CO_2$ in (A) SILM, bulk EmimNTf$_2$, (B) PES200, and PES200 filled with mineral oil. The spectrum in red is obtained by subtracting the spectrum in bulk EmimNTf$_2$ from the SILM spectrum.

intense peak at 2271 cm^{-1} along with the 2276 cm^{-1} peak observed in the bulk IL. The red curve in Figure 1A is the remaining spectrum after subtracting the scaled bulk IL CO_2 spectrum (blue) from the total spectrum (black). This additional feature that is not present in the bulk IL or SeCN$^-$ in the SILM is assigned to $^{13}CO_2$ in the polymer itself. The amplitude ratio of the two large peaks in the SILM spectrum varies with sample in a range of 0.4 to 0.6. In addition to the two major peaks, there is a small sideband at 2266 cm^{-1} which is a hot band arising from the combination of thermally excited bend and the asymmetric stretch modes of $^{13}CO_2$ in the polymer. On the red side of the hot band, there is a very weak transition attributed to a small amount of $^{13}C^{18}O_2$ in the $^{13}CO_2$ gas. Both features were also observed in the bulk IL.[24]

Figure 1B confirms that the additional peak at 2271 cm^{-1} arises from $^{13}CO_2$ in the polymer. The black spectrum is $^{13}CO_2$ in the membrane with no IL filling the pores. The rotational spectrum of gas phase $^{13}CO_2$ in the empty pores is evident in addition to the peak at 2271 cm^{-1}. The rotational spectrum disappears when the pores are filled with mineral oil as displayed in Figure 1B (blue spectrum). Because $^{13}CO_2$ is essentially insoluble in mineral oil, it only exists in the polymer phase of the membrane with its pores filled with mineral oil. The blue spectrum is identical to the subtracted spectrum in A, which is reproduced as the red spectrum in Figure 1B. Therefore, in the SILM, CO_2 not only dissolves in the IL in the pores but also in the PES polymer. When SeCN$^-$ is dissolved in the SILM, there is a single peak, corresponding to SeCN$^-$ in the bulk as an anion will have negligible solubility in the polymer. In contrast to SeCN$^-$, CO_2 is not charged or polar and can occupy free volume in the polymer that makes up the membrane.

The observation of carbon dioxide trapped in the nonporous domain of the membrane is not surprising; dense nonporous polymeric membranes have been used for gas separation

DOI: 10.1021/jacs.7b05759
J. Am. Chem. Soc. 2017, 139, 11222–11232

applications.[40] The gas transport mechanisms involved in the separation processes in the nonporous membranes is described by a solution-diffusion mass transfer model.[40] In this model, gas transport through polymer proceeds with three steps: (1) preferential gas sorption on the feed side of the membrane, (2) diffusion through the membrane driven by the concentration gradient or partial pressure difference, and (3) gas desorption on the far side of the membrane. Therefore, the product of solubility and diffusivity determines the permeability that is a measure of the membrane's ability to permeate a gas. In general, the solution-diffusion model is also applied to the liquid membranes including SILMs that are prepared with the porous membranes.[17] Thus, the PES SILM studied here can have two transport phases consisting of the IL in the pores and the polymer membrane (backbone) phase. The solution-diffusion process can occur through both phases. However, as shown below, CO_2 dynamics in the SILM is so much faster in the IL than in the polymer that transport through the polymer should make a negligible contribution to the overall transport through the SILM.

The spectrum of $^{13}CO_2$ in the SILM pores is identical to its spectrum in the bulk within experimental error. The average pore size of PES200 was measured to be ~350 nm with a broad distribution although the nominal pore size specified by the manufacturer is 200 nm.[29] Because the pores are so large, a negligible fraction of the CO_2 will be in contact with pore walls. The absorption spectrum is sensitive to the relatively local interactions between the IL and CO_2. The fact that the spectrum of $^{13}CO_2$ in $EmimNTf_2$ in the membrane pores is the same as it is in the bulk IL, within experimental error, indicates that the local structure of the IL in the pores is little different from its structure in the bulk liquid. Compared to other nanoconfined systems, such as H_2O in AOT reverse micelles in which bulk-like spectra occur away from the interface for water nanopools diameters greater than ~5 nm,[30,31] the pore dimension of PES200 are very large. Therefore, it is not surprising that the spectra of CO_2 in the bulk IL and in the membrane are the same. However, as shown below, the dynamics of the IL and CO_2 in the SILM pores are very different from those in the bulk liquid.

In the SILM sample, the asymmetric stretch band of $^{13}CO_2$ in the supporting membrane phase is red-shifted by 6 cm^{-1} from that in the IL phase. Previously, it was observed that the same $^{13}CO_2$ band in the nonpolar solvent, n-hexadecane, is red-shifted by 7 cm^{-1} from that in the bulk $EmimNTf_2$.[26] The 6 cm^{-1} red shift in the supporting membrane phase, which is comparable to the 7 cm^{-1} red shift in *n*-hexadecane, suggests that poly(ether sulfone) provides CO_2 molecules with nonpolar environment. However, the full-width at half-maximums (fwhm's) are not the same. A Voigt fit to the asymmetric stretch bands of $^{13}CO_2$ in the supporting membrane phase yields a fwhm of 5.1 compared to 7.7 cm^{-1} in *n*-hexadecane, suggesting a relatively narrower range of environments in the polymer than in the alkane.

3.2. PSPP Measurements: Population Dynamics.

Figure 2 displays the population relaxation of the asymmetric stretch of $^{13}CO_2$ in the IL in the membrane pores (blue points) and in the membrane polymer (red points). Both curves fit well to a single exponential function when the fits are begun at t = 50 ps. The results are 61 ± 2 ps for $^{13}CO_2$ in the IL in the pores (2277 cm^{-1} band) and 54 ± 2 ps for $^{13}CO_2$ in the membrane polymer (2271 cm^{-1} band). The error bars come from the variations in the results of a number of data sets taken on

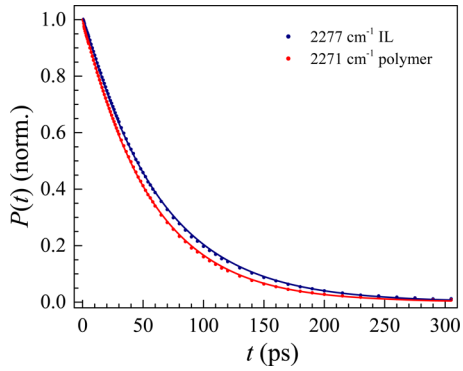

Figure 2. Population decay curves of the asymmetric stretch of $^{13}CO_2$ in the IL (2277 cm^{-1} band) and supporting membrane phases (2271 cm^{-1} band) of the SILM sample. The solid curves are the kinetic model fit described in ref 22.

different samples. The decay constant in the bulk IL starting at 50 ps is 64 ± 2 ps,[24] which is within the error bars for $^{13}CO_2$ in the IL in the membrane pores. The time constant for vibrational relaxation is sensitive to the immediate environment of the vibrational chromophore. Vibrational relaxation requires the energy in the initially excited mode to flow into a combination of lower frequency modes that conserve energy.[41,42] Generally, these will be a combination of intramolecular modes and one or modes of the bath continuum of low frequency intermolecular modes.[41] Then the difference in the lifetime for $^{13}CO_2$ in the IL and in the polymer is caused by differences in the local environments, which will have a different distribution of intermolecular modes and different couplings between the initially excited asymmetric stretch and the bath modes.

When the single exponential fits obtained at t > 50 ps for both $^{13}CO_2$ in the IL and in the polymer are extended back to t = 0, the curves are above the short time data. This behavior has been observed previously for $^{13}CO_2$ in bulk $EmimNTF_2$.[24] As shown in Figure 1A, to the red of the main bands is a hot band that is the result of the thermal population of the bending modes. When a bending mode is thermally populated, the frequency of the stretch is shifted to the red (combination band shift). The bandwidth of the IR pulses is substantially larger than the difference in frequency between the stretch and the combination band, so the excitation pulses populates both modes. When the thermally excited bend relaxes to the ground state, population is transferred from the combination band to the stretch band. When a bend becomes thermally excited, population is transferred from the stretch band to the combination band. However, the combination band has a larger transition dipole than the stretch.[24] Therefore, the small combination band is over populated relative to the thermal equilibrium ratio of populations, and there will be a net flow of population from the combination band to the stretch band. After several bend lifetimes, the excited state populations of the two bands will be in their thermal equilibrium ratio. After that, population exchange will continue, but it will not influence the long time (>50 ps) exponential lifetime decay of the stretch band.

In addition to influencing the population decays, population exchange between the hot band and the stretch band produces off-diagonal peaks that grow in with the bend lifetime.[24] This process has been discussed in detail for $^{13}CO_2$ in the bulk IL.[24] The only difference here is that there are two sets of off-

DOI: 10.1021/jacs.7b05759
J. Am. Chem. Soc. 2017, 139, 11222−11232

diagonal peaks, one set involving the $^{13}CO_2$ in the IL in the membrane pores and the other set involving the $^{13}CO_2$ in the membrane polymer. Within experimental error, the bend lifetimes in both membrane environments are the same as found in the bulk IL, 13 ps. This very low amplitudes off-diagonal peaks do not influence the analysis of the diagonal peaks to give the time dependence of the spectral diffusion and the FFCF.

Within the experimental error, the $^{13}CO_2$ asymmetric stretching mode lifetime is the same in the IL in the membrane pores as it is in the bulk IL. The lack of change in the vibrational lifetime in the SILM pores was also observed in the study of the same SILM with $SeCN^-$ as the vibrational probe.[29] As discussed briefly above, vibration relaxation is very sensitive to the local environment. The fact that the vibrational lifetimes are the same in the bulk and in the pores for two vibrational probes indicates that there is no substantial change in the structure of the IL surrounding the probes.

3.3. PSPP Measurements: Reorientation Dynamics. The anisotropy data from the PSPP measurements were utilized to determine the orientational relaxation of the $^{13}CO_2$ (see eq 4). Figure 3 presents the anisotropy decays of $^{13}CO_2$ in the bulk EmimNTf$_2$, in the IL in the SILM pores, and in the membrane polymer. The data were taken at the center frequency of each of the asymmetric stretch bands. All of the anisotropy decays in Figure 3 begin with initial values less than the maximum anisotropy value, 0.4, when the data are extrapolated back to $t = 0$. This initial drop from 0.4 is caused by ultrafast inertial orientational motion that occurs on a faster time scale than the time duration of the overlapped pulses and cannot be resolved.[43] The difference between 0.4 and the $t = 0$ value gives information on the extent of inertial orientational motion. After the initial drop, the anisotropy curves are fit well by triexponential decays (Figure 3), and their fit parameters are summarized in Table 1. No offsets are needed in the fits of the anisotropy decays for the $^{13}CO_2$ in EmimNTf$_2$ in the SILM pores and the bulk sample, indicating that there is complete orientational relaxation. In contrast, for $^{13}CO_2$ in the polymer of the SILM, an offset is necessary in their fits because the time range in which the data can be collected is limited by the vibrational lifetime and is not long enough to determine the complete anisotropy curve. It is difficult to determine the offset level in the fit, which results in a large error in the longest time constant, t_3. If the offset is fixed to 0 in the fit, the first two time constants do not change, but t_3 becomes very long, well outside the experimental range but has a smaller error because the long time constant and the offset do not play off against each other. As will be discussed below, the 2D IR experiments suggest that the $^{13}CO_2$ ensemble in the polymer is unlikely to undergo complete orientational randomization. The 2D IR data led to fitting the anisotropy data from the membrane phase with a triexponential decay with an offset. With either fitting procedure, it is clear that the final complete orientation relaxation either does not occur or it is exceedingly slow.

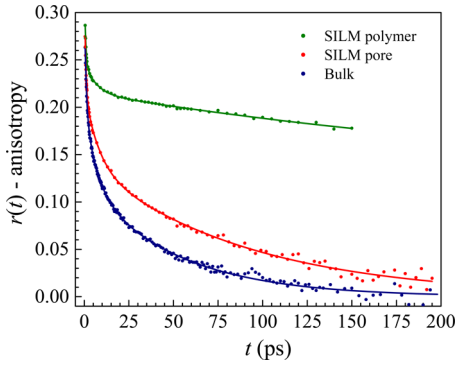

Figure 3. Anisotropy decay curves of $^{13}CO_2$ in the bulk EmimNTf$_2$ and the IL and supporting membrane phases of SILM. The solid curves are triexponential fits to the data.

As depicted in Figure 3, the anisotropy decays of $^{13}CO_2$ slows down in the IL in the pores and in the polymer. In going from the bulk sample to the IL phase in the SILM, the longest time constant, t_3, changes from 51 to 90 ps while the first two time constants, t_1 and t_2, remain unaffected within experimental error.

The triexponential anisotropy decays in EmimNTf$_2$ for both the bulk and in the IL in the SILM samples, after the inertial drop, can be interpreted as two sequentially restricted angular diffusions (wobbling-in-a-cone) followed by complete orientational randomization of the $^{13}CO_2$.[44−47] Using the standard approach (wobbling analysis),[44,45,48,49] the cone angles are retrieved from the amplitudes of the exponential terms in the anisotropy decay, and the correlation times are given by $\tau_{c1} = t_1$ for the first cone, $\tau_{c2} = (1/t_2 - 1/t_3)^{-1}$ for the second cone, and $\tau_m = t_3$ for the complete orientational randomization. The orientational diffusion constants for each cone are calculated based on both cone angle and correlation time.[44] The inertial cone angle is recovered from the extent of the initial drop, but its time dependence cannot be resolved. The resulting parameters from the wobbling analysis are tabulated in Table 2. The inertial cone angle of the IL phase in the SILM sample is somewhat smaller than that in the bulk sample. The local IL structure in the SILM allows $^{13}CO_2$ to have smaller space available for ballistic inertial motion than in the bulk sample. This is an indication that the IL structure surrounding the $^{13}CO_2$ is not identical to the bulk liquid, in contrast to the spectra and lifetimes, which were not changed within experimental error. The second cone angle in the pores is also slightly smaller compared to the bulk sample whereas the first cone angles in the both samples are almost the same. The decrease in both inertial and second cone angles of the SILM sample leads to the decrease in the total cone angle that is sampled prior to the complete orientational randomization. However, the overall differences in the cone angles between the bulk and SILM samples are small; there is only subtle change in

Table 1. Parameters from the Triexponential Fits to the Anisotropy Decays

sample	A_1[a]	t_1 (ps)	A_2[a]	t_2 (ps)	A_3[a]	t_3 (ps)	offset
bulk	0.11 ± 0.01	0.9 ± 0.1	0.08 ± 0.01	6.5 ± 0.7	0.12 ± 0.01	51 ± 1	0
SILM (pore)	0.13 ± 0.01	0.6 ± 0.1	0.08 ± 0.01	7.5 ± 0.9	0.14 ± 0.01	90 ± 2	0
SILM (polymer)	0.10 ± 0.01	0.6 ± 0.1	0.03 ± 0.01	6.1 ± 0.6	0.10 ± 0.03	309 ± 119	0.12 ± 0.03

[a] A_i is the amplitude of each exponential.

DOI: 10.1021/jacs.7b05759
J. Am. Chem. Soc. 2017, 139, 11222−11232

Table 2. Parameters from Wobbling Analysis

sample	θ_{in} (deg)[a]	θ_{c1} (deg)[b]	θ_{c2} (deg)[b]	θ_{tot} (deg)[c]	τ_{c1} (ps)[d]	τ_{c2} (ps)[d]	τ_m (ps)[d]	D_{c1} (10^{-2} ps^{-1})[e]	D_{c2} (10^{-2} ps^{-1})[e]
bulk	22.5 ± 1.5	30.3 ± 0.9	33.3 ± 0.8	48.7 ± 0.5	0.9 ± 0.1	7.4 ± 0.9	51 ± 1	8.2 ± 1.4	1.2 ± 0.1
SILM (pore)	16.6 ± 2.7	31.5 ± 1.3	30.4 ± 0.7	45.5 ± 0.4	0.6 ± 0.1	8.2 ± 1.1	90 ± 2	12.9 ± 2.3	0.9 ± 0.1

[a]The inertial cone angle. [b]θ_{c1} and θ_{c2} are the first and second diffusive cone half angles. [c]The total cone half angle accounting for all three cones. [d]τ_{c1}, τ_{c2}, and τ_m are the decay times associated with the first and second diffusive cones and the final free diffusion, respectively. [e]D_{c1} and D_{c2} are the first and second cone diffusion constants.

the local environment experienced by $^{13}CO_2$. Within the error bars, the time constants for the first and second cones are very close for the two samples, and thus, given the small changes in the cone angles, the diffusion constants are similar. The similarities in the cone angles, correlation times, and diffusion constants reflect that the local environments around $^{13}CO_2$ are very similar in the pores and bulk sample. This is consistent with the previous results, using $SeCN^-$ as the probe, that the local IL structure is essentially unaffected by confinement in the pores of the PES200 membrane.[29]

Unlike the wobbling-in-a-cone, the time constant for the complete orientational randomization, τ_m, increases from 51 to 90 ps in going from the bulk to the SILM sample, revealing significant slowdown. (The diffusion constant is $D_m = 1/6\tau_m$.) In the previous study, it was found that τ_m of $^{13}CO_2$ in the bulk $EmimNTf_2$ agrees well with the orientational diffusion time constant calculated from the Debye−Stokes−Einstein (DSE) equation under the slip boundary conditions.[25] In addition, τ_m increased in proportion to the viscosity of the bulk IL as the alkyl chain of the cation of the IL became longer.[26] This suggests that the rearrangement of global IL structure is necessary for CO_2 to undergo the complete orientational randomization and for the bulk ions to move out of the way. Therefore, the increase of τ_m in the SILM sample suggests that the global IL structure is substantially influenced by the confinement in the membrane pores.

The confinement effects on the IL in the PES200 membrane as shown through the deviation from the bulk liquid dynamics were unexpected because the pore size is very large compared to the sizes of other systems where nanoconfinement strongly affects liquid dynamics.[30,31,50−52] The IL structure at surfaces and interfaces has been of great interest recently, and it is commonly accepted that the interactions with interfaces can affect the ordering of cations and anions within a few nanometers from interfaces.[53−59] However, this picture has been challenged by recent experimental and theoretical studies which indicate that ILs can form ordered structures distinct from the bulk over much large distances from an interface.[60−63] In line with these recent studies, our results provide substantial evidence that the poly(ether sulfone) interface can influence the global IL structure over a large distance.

The slowdown of complete orientational relaxation in the SILM was also observed with $SeCN^-$ as the vibrational probe. In going from the bulk $EmimNTf_2$ to the same SILM studied here, τ_m of $SeCN^-$ increased from 136 to 512 ps.[29] This 3.8-fold increase is substantially larger than 1.8-fold increase observed here for CO_2. The similar trend also can be found in alkyl chain length dependence of τ_m. As the IL changed from $EmimNTf_2$ to $DmimNTf_2$ (1-decyl-3-methylimidazolium bis-(trifluoromethylsulfonyl)imide), τ_m increased by a factor of 3.6 for $SeCN^-$ and 1.8 for CO_2.[26,27] The carbon dioxide molecule is relatively small and is known to occupy empty cavities in the IL.[64] In addition, CO_2 is a neutral molecule, mainly interacting with anions in the IL[65,66] whereas $SeCN^-$ is an anion, probably interacting more strongly with cations in the IL.

To qualitatively address the extent of the slowing of the IL rearrangement experienced by CO_2 in the SILM, an "effective viscosity" can be determined. With the reasonable assumption that the shape and volume of CO_2 does not change when confined in the SILM, τ_m only depends on the viscosity according to the DSE equation. However, the alkyl chain length dependent experiments with the $^{13}CO_2$ vibrational probe found that τ_m does not perfectly follow the bulk viscosity changes.[26] To compensate for this difference, a correlation plot of τ_m measured in different IL versus the bulk viscosity of each IL was fit with linear functional form to obtain the empirical relationship. Then, the effective viscosity experienced by CO_2 in the SILM can be obtained using τ_m of the SILM sample and the empirical functional form. The calculated effective viscosity in the SILM is 117.0 cP which is close to the bulk viscosity of $DmimNTf_2$ (134.4 cP).[26] The viscosity of bulk $EmimNTf_2$ is 36.3 cP. The effective viscosity of the IL in the pores is ∼3 times greater than the bulk viscosity. This increase in the viscosity is quite remarkable because CO_2 is in the same IL in both bulk and SILM samples and only difference is the presence of polymer interface in the SILM sample. The long-range IL ordering effect caused by the pore interfaces substantially influences the global IL dynamics.

3.4. 2D IR Measurements: Spectral Diffusion and Structural Dynamics. 2D IR spectroscopy measures structural evolution of a system by reporting on the spectral diffusion of a vibrational probe that senses the dynamics of surrounding liquid structures. The vibrational probe molecules will experience different interactions with their surroundings because of the inhomogeneity in the liquid structures, giving rise to the inhomogeneous broadening of the vibrational absorption line. Spectral diffusion provides information on how long it takes the probe molecules to sample all the frequencies in the inhomogeneously broadened line, i.e., all the liquid structures that contribute to inhomogeneous broadening of the absorption spectrum. The amplitudes and time scales of the spectral diffusion can be quantified through the FFCF, which is the probability that a vibrational oscillator with an initial frequency in the inhomogeneous spectral distribution will have that same frequency at a later time, averaged over all initial frequencies. The FFCF is modeled with a multiexponential form

$$C(t) = \langle \delta\omega(t)\delta\omega(0)\rangle = \sum_i \Delta_i^2 \exp(-t/\tau_i) \quad (5)$$

where Δ_i and τ_i are the frequency fluctuation amplitudes and associated time constant, respectively, for the ith component. $\delta\omega(t) = \omega(t) - \langle\omega\rangle$ is the instantaneous frequency fluctuation, where $\langle\omega\rangle$ is the average frequency. A component of the FFCF is motionally narrowed if $\Delta\tau < 1$, and then its Δ and τ cannot be determined separately. The motionally narrowed component contributes to the homogeneous broadening of the

DOI: 10.1021/jacs.7b05759
J. Am. Chem. Soc. 2017, 139, 11222−11232

absorption line and has a pure dephasing line width, given by $\Gamma^* = \Delta^2\tau/\pi = 1/(\pi T_2^*)$, where T_2^* is the pure dephasing time. The vibrational lifetime and orientational relaxation also contribute to the homogeneous broadening through the total homogeneous dephasing time, T_2 which is given by

$$\frac{1}{T_2} = \frac{1}{T_2^*} + \frac{1}{2T_1} + \frac{1}{3T_{or}} \quad (6)$$

where T_1 and T_{or} are the vibrational lifetime and orientational relaxation time, respectively. Then, the total homogeneous line width is $\Gamma = 1/(\pi T_2)$. As mentioned in the Experimental Procedures, the FFCF can be extracted from the line shape analysis of 2D IR spectra, using the CLS method.[38,39]

Figure 4 presents 2D IR spectra of $^{13}CO_2$ in the SILM sample at T_w = 4 and 60 ps. Two diagonal bands are from two

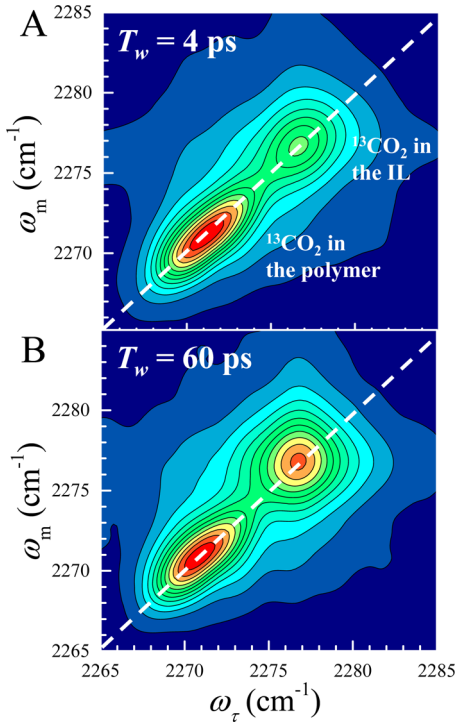

Figure 4. 2D IR spectra of the asymmetric stretch of $^{13}CO_2$ in SILM. (A) The spectrum at short waiting time. The bands from both the IL and supporting membrane phases are elongated along the diagonal, the dashed line. (B) The spectrum at longer waiting time. The supporting membrane phase band at 2271 cm^{-1} is fairly elongated while the IL phase band at 2277 cm^{-1} looks almost round. The spectral diffusion is obtained from the change in shape of the spectrum with T_w.

ensembles of $^{13}CO_2$ residing in the IL and the polymer that makes up the membrane. At a short waiting time, T_w = 4 ps (Figure 4A), both bands are elongated along the diagonal (dashed white line) because the environment has had little time to evolve and the vibrational oscillators have frequencies close to their initial frequencies. However, the extent of elongation for each band is different, with $^{13}CO_2$ in the polymer having a higher degree of elongation than that for $^{13}CO_2$ in the IL in the membrane pores. At a longer waiting time, T_w = 60 ps (Figure 4B), the shape of IL phase band becomes more round due to the evolution of IL structures. In contrast, the band shape of the supporting membrane phase is not very different from the initially elongated shape at T_w = 4 ps, indicating its slow spectral diffusion. Note that the spectra are normalized to the highest amplitude contour. In Figure 4B, the IL band has become relatively higher in amplitude because it has a longer lifetime. At very long time, the IL band is larger in amplitude than the polymer band.

As discussed in the Experimental Procedures, 2D IR experiments were performed in ⟨*XXXX*⟩ (parallel) and ⟨*XXYY*⟩ (perpendicular) polarization configurations. It was recently observed that the CLS decays obtained with these two polarization configurations are not necessarily the same, demonstrating that, in certain cases, structural fluctuations of the sample medium do not entirely determine the frequency fluctuations of the vibrational probe.[67] The rotation of the molecule can also play a role. The difference in the parallel and perpendicular decay curves was addressed by modeling the interaction of the vibration with its surroundings as coupling to electric fields, Stark effect, produced by the liquid in which the vibrational probe is embedded. For CO_2, the coupling is through the second order Stark effect.[25,67,68] When the field varies on a similar time scale, or slowly, relative to the orientational relaxation times of the probe molecule, frequency fluctuations occur due to the probe rotation. Therefore, reorientation of the probe molecule contributes to spectral diffusion and gives rise to different CLS decays for ⟨*XXXX*⟩ and ⟨*XXYY*⟩ polarization configurations.[25,67,68] This phenomenon is referred to as reorientation-induced spectral diffusion (RISD), in contrast to structural spectral diffusion (SSD), which arises solely from structural evolution of the liquid. In general, we are interested in measuring SSD. Analytical expressions are available for the RISD contribution. The expressions use the orientational relaxation measured with PSPP experiments as their inputs. Therefore, the SSD can be obtained from fitting the parallel and perpendicular 2D IR data. The second-order Stark effect RISD theory for CO_2 results a further separation of SSD into the contributions from scalar and vector interactions of the medium with CO_2. A more detailed discussion including the equations used in the data fitting are presented in Supporting Information.

Figure 5A shows 2D IR CLS data (points) for both the bulk sample and the IL in the membrane pores in the ⟨*XXXX*⟩ and ⟨*XXYY*⟩ polarization configurations. The data for each sample are simultaneously fit with the second-order Stark model described briefly above. The scalar and vector correlation functions were modeled with the same functional forms as previously used for the bulk sample:[25,26] a biexponential for the scalar part and a single exponential for the vector part. The model fits the data very well, as can be seen in Figure 5A (solid lines). If single exponentials are used for each term, the model does not fit the data. In addition, adding more exponentials does not improve the fit quality and does not result in unique time constants.

In the SILM sample, ⟨*XXXX*⟩ CLS curve of IL phase band (2277 cm^{-1}) showed a small oscillatory feature starting with growth at short waiting time from 0.3 ps up to 3 ps. The same feature starting with decay also appeared in its ⟨*XXYY*⟩ CLS. (The features are not shown here.) The oscillations in CLS curves have previously been observed in D_2O in RTIL. The coherent energy transfer between symmetric and antisymmetric stretch modes of D_2O can cause the oscillations in the 2D line shapes.[69] The oscillatory feature observed in the SILM sample could also indicate the presence of the coherent excitation transfer, presumably between asymmetric stretch mode of CO_2 and its hot band; the beating pattern appears differently in two

DOI: 10.1021/jacs.7b05759
J. Am. Chem. Soc. 2017, 139, 11222−11232

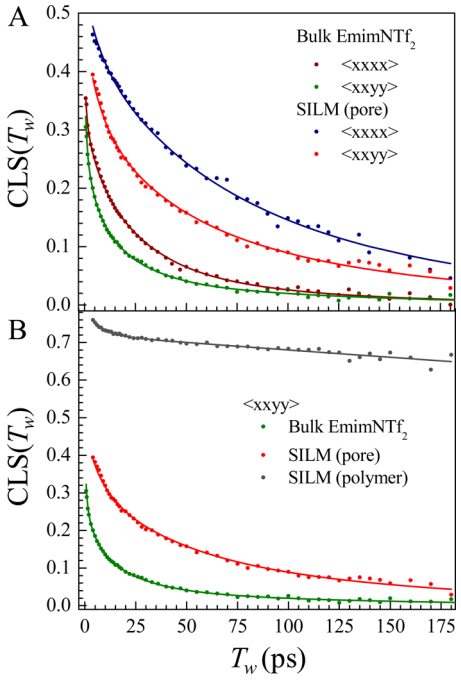

Figure 5. 2D IR CLS (normalized frequency-frequency correlation function) decay data of $^{13}CO_2$ (A) in the bulk EmimNTf$_2$ and IL phase of SILM (2277 cm^{-1}) from both the parallel and perpendicular polarization configurations and (B) in the bulk EmimNTf$_2$ and the IL (2277 cm^{-1}) and supporting membrane phases (2271 cm^{-1}) of SILM from the perpendicular polarization configuration. The solid curves are the second-order RISD fits to the data, except for the supporting membrane phase data which are fit with biexponential.

polarization configurations. Another possibility is that there is a fast rapidly damped physical oscillation of the CO_2 relative to the anions it interacts with. This type of oscillation has been observed HOD in D_2O at very short times (~100 fs)[70] and on a longer time scale (1.5 ps) for benzonitrile in a metal organic framework.[71] As the oscillation is not observed in the bulk sample, the second explanation may be correct and indicate a difference in the CO_2−IL interaction in the membrane pores compared to the bulk IL. However, the exact origin is unclear. For this reason, the early time CLS points up to 4 ps were excluded in the RISD fit for the SILM sample. Since the time scales of CLS decays are significantly longer than that of early time features, the results from the RISD fit will not be affected. Table 3 summarizes the SSD parameters obtained from the second-order Stark model fits, comparing CO_2 in the bulk EmimNTf$_2$ and in the IL phase of SILM sample.

As can be seen in Figure 5A, the CLS decays of CO_2 in the IL phase are substantially slower in the SILM sample. In going from the bulk to SILM samples, the longer time constant, τ_2, in the scalar correlation function and the vector correlation time, τ_3, increase by a factor of 2 while the shorter time constant, τ_1, in the scalar part remains the same as found for the bulk, within the error bars. The similar changes in the τ_2 and $\tau_3$time scales in going from the bulk IL to IL in the pores may suggest that both time constants originate from the same IL motions that can alter both the magnitude and direction of the solvent's internal electric fields. In contrast, the short scalar correlation time, τ_1, is unchanged in going from the bulk to the pores. This component was previously observed to display no dependence on the alkyl chain length of bulk RTILs, which suggests its insensitivity to the extent of nonpolar aggregation of the IL and thus, the overall IL structures.[26] It may involve very local IL motions that are not influenced by either alkyl chain length or confinement in the membrane pores.

In contrast, it was observed that the two SSD components, τ_2 and τ_3, are sensitive to the global structures and overall fluctuations of IL.[26] In the CO_2 study in the bulk RTILs, τ_2 and τ_3 became longer with increasing alkyl chain length of IL. The chain length dependence in the bulk indicates that the slowdown in τ_2 and τ_3 in the SILM sample reflects a change in the global IL structure and their dynamics. The slowing of the spectral diffusion and the slowing of the orientational relaxation in the SILM relative to the same IL in the bulk demonstrates that the IL dynamics, and therefore structure, is significantly influenced by the presence of the pore interface, in spite of the large pore sizes. The same trend in SSD was observed for the $SeCN^-$ in SILM.[29]

Although the polarization dependent CLS data allows us to determine the SSD part of the total FFCF without the RISD contributions, MD simulations will determine the complete FFCF without a separation into SSD and RISD components.[72] Therefore, the isotropic decay is obtained by taking the parallel 2D spectrum and adding twice the perpendicular spectrum with the parallel and perpendicular spectra properly normalized. The resulting isotropic curve, which still contains the RISD contribution, is useful because it is the CLS that would be calculated in a molecular dynamics (MD) simulations, which in general, do not include the polarized radiation fields. The isotropic FFCF parameters obtained from the isotropic CLS decays are given in Table 4.

In contrast to the IL CLS data of the SILM and the bulk, the membrane phase data did not yield data that is consistent with the RISD theory. The parallel and perpendicular measurements on $^{13}CO_2$ in the polymer did not show the characteristic behavior in which the perpendicular decay is faster than the parallel decay. The RISD theory was derived for vibrational probes that are orientationally distributed randomly relative to the electric fields produced by the surrounding medium. If the CO_2 enters the polymer strands with an orientation that is correlated with the strand topography and it does not undergo complete rotational relaxation, then it is likely that the CO_2 will not be randomly oriented relative to the polymer produced electric field. This is a situation that is not covered by the RISD theory. As discussed in connection with the orientational relaxation of CO_2 in the polymer, there is a very slow component. The slow component is either an offset, which

Table 3. SSD Parameters from RISD Fits Based on the Second-Order Stark Effect Model

	F_s, scalar correlation				F_v, vector correlation	
sample	A_1[a]	τ_1 (ps)	A_2[a]	τ_2 (ps)	A_3[a]	τ_3 (ps)
IL bulk	0.09 ± 0.02	20 ± 5	0.07 ± 0.02	77 ± 20	0.36 ± 0.01	57 ± 5
IL in pores	0.04 ± 0.01	17 ± 8	0.17 ± 0.01	143 ± 11	0.54 ± 0.01	113 ± 7

[a] A_i is the amplitude of each exponential.

DOI: 10.1021/jacs.7b05759
J. Am. Chem. Soc. 2017, 139, 11222−11232

Table 4. Isotropic FFCF Parameters

sample	Γ (cm^{-1})[a]	Δ_1 (cm^{-1})[b]	τ_1 (ps)[c]	Δ_2 (cm^{-1})[b]	τ_2 (ps)[c]
IL bulk	3.2 ± 0.1	0.99 ± 0.02	7.2 ± 1.2	0.95 ± 0.05	52 ± 4
IL in pores	2.7 ± 0.2	0.98 ± 0.04	14.2 ± 1.9	1.12 ± 0.06	82 ± 12

[a]Γ: homogeneous line width (fwhm). [b]Δ_i: inhomogeneous line width (standard deviation) of the ith component. [c]τ_i: decay time constant of the ith component.

means that complete orientational relaxation does not occur, or it is a very slow component. However, a very slow component, even if it is much slower than the vibrational lifetime, will still result in random orientations of the CO_2 relative to the polymer, in which case the RISD theory should work. Vibrational probes that are coupled to electric fields by either first or second order Stark effects have displayed the features described by RISD theory for a wide variety of systems.[25−28,67,68] Therefore, it is likely that the CO_2 does not undergo complete orientational relaxation in the polymer.

While RISD theory cannot be applied to separate SSD and RISD, we can still compare the spectral diffusion of CO_2 in the polymer vs the bulk IL and the IL in the membrane pores. Figure 5B shows the perpendicular data sets for the three environments, CO_2 in the bulk IL, in the IL in the pores, and in the polymer. The structural dynamics in the polymer is vastly slower than in either the bulk IL or the IL in the pores. As the main interest is the difference in the dynamics in the IL in the pores vs in the bulk IL, no further analysis of dynamics of CO_2 in the polymer will be given.

Comparison of the CO_2 SSD for the bulk and IL in the pores shows that spectral diffusion in the pores is substantially slower than in the bulk. The comparison of the orientational relaxation displays the same behavior. The interfaces of pores induce the reconfigurations of IL's global structures, presumably through the long-range ordering effect, slowing down the dynamics. In the membrane phase of SILM, the spectral diffusion of CO_2 is far slower due to the direct interactions with the polymer.

3.5. Estimate of Translational Diffusion in the Pores. For practical application as a carbon capture material, the ability of CO_2 to diffuse through the SILM, that is diffusivity, is one of important factors together with solubility.[17] An estimate of the translational diffusion in the pores can be made using the effective viscosity given above. If the molecular motions are reasonably hydrodynamic, both rotational and translational diffusion will be governed by the same friction term. In cases where the solute molecule is relatively small compared to the solvent, like CO_2 in the IL, then both rotational and translational diffusion will have slip boundary conditions rather than stick. The standard form of the Stokes−Einstein (SE) equation is for stick boundary conditions and spherical particles. With slip boundary conditions, diffusion occurs more rapidly than predicted by the standard SE equation.[32]

The standard SE equation for diffusion can be modified for a small and nonspherical molecule by including a shape factor and size factors in the equation.[32,33] A modified SE equation gives the translational diffusion constant as

$$D_T = \frac{k_B T}{c\pi r \eta f} \tag{7}$$

where k_B is Boltzmann's constant, T is absolute temperature, and η is the viscosity. $r = 3/(4\pi) \times V_{eff}^{1/3}$ is the effective radius, where V_{eff} is the molecular volume. The size factor, c, accounts the relative hydrodynamic dimensions of the diffusing species and solvent and can be derived from the microfriction theory.[73] The shape factor, f, is used for the nonspherical diffusing particles and has been theoretically calculated for prolate and oblate ellipsoids.[74] If we assume that none of the molecular properties change in going from the bulk IL to the IL in the pores, i.e., the molecular dimensions, the CO_2 shape factor, then the diffusion constant in the IL pores is determined by the ratio of the viscosity for the bulk IL (36.3 cP) and the effective viscosity determined from the orientation relaxation time for the IL in the pores (117 cP). The experimental value in the bulk IL is 5×10^{-6} cm^2s^{-1}.[75,76] Then, the estimated value for the IL in the SILM pores is 1.6×10^{-6} cm^2s^{-1}.

Although there is no experimentally determined diffusion constant that can be directly compared, the diffusivity can be extracted from the permeability of CO_2 measured in the same SILM. Scovazzo et al. have measured the CO_2 permeability through the SILM prepared with PES200 and $EmimNTf_2$, using the time-lag method in gas flux experiments.[77] Because the permeability is a product of solubility and diffusivity according to the solution-diffusion model,[17] the diffusivity can be calculated based on the reported permeability (960 barrers) and CO_2 gas solubility in the bulk $EmimNTf_2$ (0.1 mol/L atm).[77] It should be noted that the CO_2 solubility used in this calculation is for the bulk $EmimNTf_2$, not for the SILM. The value for the SILM is unavailable in the literature. The calculated diffusivity, 3.2×10^{-6} cm^2s^{-1}, is larger than the diffusion constant obtained from the effective viscosity determined using the orientational relaxation measurements by a factor of 2. In the permeability experiments, a pressure gradient is applied across the SILM to drive the diffusion of CO_2 in the gas flux measurements.[32] The presence of driving force can accelerate the diffusion of CO_2, which results in larger diffusion constant. Another possibility is that the CO_2 solubility in the SILM might be larger than that in the bulk IL. A recent simulation study demonstrated that nanoconfinement of IL in model membranes with very small 2 and 5 nm pores increases CO_2 solubility compared to the bulk IL.[78] Although the pore sizes in the simulation are much smaller than the SILM used in this study, the solubility could still be affected by the confinement in the SILM as the CO_2/IL dynamics are influenced. Nonetheless, both the permeability measurements and the orientational relaxation measurements indicate that the translational diffusion in the IL in the pores is slower than in the bulk IL, presumably because of the long-range IL ordering caused by the pore interface.

4. CONCLUDING REMARKS

The dynamics of $^{13}CO_2$ in a SILM prepared with $EmimNTf_2$ and PES200 polymer membranes were investigated by the polarization selective pump−probe and 2D IR spectroscopies and compared to the corresponding bulk sample. The FT-IR spectrum of $^{13}CO_2$ in the SILM sample showed a bulk-like absorption bands and an additional band that is red-shifted by 6 cm^{-1} from the bulk IR absorption spectrum. Since the red-shifted band was observed in the $^{13}CO_2$ samples in PES200 with and without the IL in the pores (Figure 1), the additional

DOI: 10.1021/jacs.7b05759
J. Am. Chem. Soc. 2017, 139, 11222−11232

features in the SILM sample can be assigned to the CO_2 in the polymer that makes up the membrane. The population data analysis found that the lifetimes of asymmetric stretch mode are the same in the bulk IL and in the IL in the SILM pores but the lifetime is shorter in the polymer. The facts that the $^{13}CO_2$ spectra and the lifetimes in the bulk IL and the IL in the pores are the same, demonstrate that there is no major difference in the very local environment surrounding the $^{13}CO_2$.

The orientational relaxation anisotropy decays showed substantial differences between the bulk IL and IL in the membrane samples. For the CO_2 in the IL phase in the bulk and SILM samples, the anisotropy decays were analyzed by the wobbling-in-a-cone model. While the half angles and time constants for two wobbling cones were similar in the bulk and pores, the complete orientational relaxation time increased by a factor of ~2 in going from bulk to SILM. The effective viscosity that CO_2 experiences in $EmimNTf_2$ confined in the SILM pore was found to be 117.0 cP compared to the bulk viscosity of 36.3 cP. The translational diffusion constant of CO_2 in SILM was found approximately using the effective viscosity. The value of 1.6×10^{-6} cm^2s^{-1} is approximately a factor of 3 smaller than the value in the bulk.

The slowing of the dynamics in SILM was also demonstrated by polarization selective 2D IR experiments. Like the anisotropy decays, the fastest components of the spectral diffusion in the bulk IL and in the IL in the pores are the same within error. However, the slower two components are slower in the pores than in the bulk by a factor of ~2. Both the anisotropy data and the 2D IR data taken on the absorption band corresponding to CO_2 in the polymer show dramatic slowing compared to CO_2 in the IL. Given that the polymer is a solid, this is not surprising. Experiments that cannot discriminate between CO_2 in the IL in the pores and in the polymer may need to consider that there are two distinct subensembles of CO_2 in the membrane that have very different dynamics.

CO_2 in the PES200 SILMs like a previous study of $SeCN^-$ in the same SILM[29] shows that the influence of confinement in the pores is significant. The pores in these membranes have an average diameter of ~350 nm.[29] This diameter is large, approaching macroscopic size. Other types of liquids in pores of this size would not show confinement effects. Only molecules very near the interface would be affected. These experiments and other experiments[53,54,56,57,59−62] and simulations[55,58,63] show that the interactions of an IL with an interface are very different from those of other liquids. ILs in the bulk always show charge ordering. The influence of the interface may be to produce charge ordering at the interface that is very different from that found in the bulk. Then strong Coulomb interactions among the ions apparently propagate this structural difference over long distances. Understanding how interfaces influence the structure and dynamics of ILs is an interesting and important topic.

Finally, the main purpose of SILMs is to capture CO_2. For practical applications, CO_2 selectivity and transport rate are important for the performance of a SILM. Then, the properties of both RTILs and supporting membranes must be tested and optimized. The results presented here demonstrate that the dynamics of ILs confined in SILMs are different from those found in the bulk IL. Long-range ordering effect near the interfaces can slow down the structural dynamics of IL and, therefore, the orientational and translational diffusions of CO_2. The properties and dynamics of ILs in SILMs cannot necessarily be predicted from the bulk IL. Then, fundamental understanding of molecular interactions of RTILs and their dynamics in SILMs is important for developing SILMs for application in CO_2 capture.

■ ASSOCIATED CONTENT

Supporting Information

The Supporting Information is available free of charge on the ACS Publications website at DOI: 10.1021/jacs.7b05759.

Details of the second-order Stark effect RISD theory (PDF)

■ AUTHOR INFORMATION

Corresponding Author

*fayer@stanford.edu

ORCID

Michael D. Fayer: 0000-0002-0021-1815

Notes

The authors declare no competing financial interest.

■ ACKNOWLEDGMENTS

This work was funded by the Division of Chemical Sciences, Geosciences, and Biosciences, Office of Basic Energy Sciences of the U.S. Department of Energy through Grant #DE-FG03-84ER13251. Additional support came from the Stanford Center for Carbon Storage, which provided partial salary support for J.Y.S.

■ REFERENCES

(1) Dlugokencky, E.; Tans, P. NOAA/ESRL: http://www.esrl.noaa.gov/gmd/ccgg/trends/ (accessed May 2, 2017).

(2) Solomon, S.; Plattner, G.-K.; Knutti, R.; Friedlingstein, P. *Proc. Natl. Acad. Sci. U. S. A.* **2009**, *106*, 1704−1709.

(3) Shakun, J. D.; Clark, P. U.; He, F.; Marcott, S. A.; Mix, A. C.; Liu, Z.; Otto-Bliesner, B.; Schmittner, A.; Bard, E. *Nature* **2012**, *484*, 49−54.

(4) Metz, B.; Davidson, O.; Coninck, H. d.; Loos, M.; Meyer, L. *IPCC Special Report on Carbon Dioxide Capture and Storage. Prepared by Working Group III of the Intergovernmental Panel on Climate Change*; Cambridge University Press: Cambridge, U.K., 2005; p 442.

(5) Haszeldine, R. S. *Science* **2009**, *325*, 1647−1652.

(6) Plechkova, N. V.; Seddon, K. R. *Chem. Soc. Rev.* **2008**, *37*, 123−150.

(7) Earle, M. J.; Esperanca, J. M. S. S.; Gilea, M. A.; Canongia Lopes, J. N.; Rebelo, L. P. N.; Magee, J. W.; Seddon, K. R.; Widegren, J. A. *Nature* **2006**, *439*, 831−834.

(8) Smiglak, M.; Reichert, W. M.; Holbrey, J. D.; Wilkes, J. S.; Sun, L.; Thrasher, J. S.; Kirichenko, K.; Singh, S.; Katritzky, A. R.; Rogers, R. D. *Chem. Commun.* **2006**, 2554−2556.

(9) Anderson, J. L.; Ding, R.; Ellern, A.; Armstrong, D. W. *J. Am. Chem. Soc.* **2005**, *127*, 593−604.

(10) Castner, E. W.; Margulis, C. J.; Maroncelli, M.; Wishart, J. F. *Annu. Rev. Phys. Chem.* **2011**, *62*, 85−105.

(11) MacDowell, N.; Florin, N.; Buchard, A.; Hallett, J.; Galindo, A.; Jackson, G.; Adjiman, C. S.; Williams, C. K.; Shah, N.; Fennell, P. *Energy Environ. Sci.* **2010**, *3*, 1645−1669.

(12) Kenarsari, S. D.; Yang, D.; Jiang, G.; Zhang, S.; Wang, J.; Russell, A. G.; Wei, Q.; Fan, M. *RSC Adv.* **2013**, *3*, 22739−22773.

(13) Boot-Handford, M. E.; Abanades, J. C.; Anthony, E. J.; Blunt, M. J.; Brandani, S.; Mac Dowell, N.; Fernandez, J. R.; Ferrari, M.-C.; Gross, R.; Hallett, J. P.; Haszeldine, R. S.; Heptonstall, P.; Lyngfelt, A.; Makuch, Z.; Mangano, E.; Porter, R. T. J.; Pourkashanian, M.; Rochelle, G. T.; Shah, N.; Yao, J. G.; Fennell, P. S. *Energy Environ. Sci.* **2014**, *7*, 130−189.

DOI: 10.1021/jacs.7b05759
J. Am. Chem. Soc. 2017, 139, 11222−11232

(14) Scovazzo, P.; Visser, A. E.; Davis, J. H.; Rogers, R. D.; Koval, C. A.; DuBois, D. L.; Noble, R. D. Supported Ionic Liquid Membranes and Facilitated Ionic Liquid Membranes. In *Ionic Liquids*; American Chemical Society: Washington, D.C., 2002; Vol. *818*, pp 69−87.
(15) Lozano, L. J.; Godínez, C.; de los Ríos, A. P.; Hernández-Fernández, F. J.; Sánchez-Segado, S.; Alguacil, F. J. *J. Membr. Sci.* **2011**, *376*, 1−14.
(16) Dai, Z.; Noble, R. D.; Gin, D. L.; Zhang, X.; Deng, L. *J. Membr. Sci.* **2016**, *497*, 1−20.
(17) Tome, L. C.; Marrucho, I. M. *Chem. Soc. Rev.* **2016**, *45*, 2785−2824.
(18) Zhang, S.; Zhang, J.; Zhang, Y.; Deng, Y. *Chem. Rev.* **2017**, *117*, 6755−6833.
(19) Hazelbaker, E. D.; Guillet-Nicolas, R.; Thommes, M.; Kleitz, F.; Vasenkov, S. *Microporous Mesoporous Mater.* **2015**, *206*, 177−183.
(20) Iacob, C.; Sangoro, J. R.; Kipnusu, W. K.; Valiullin, R.; Karger, J.; Kremer, F. *Soft Matter* **2012**, *8*, 289−293.
(21) Nayeri, M.; Aronson, M. T.; Bernin, D.; Chmelka, B. F.; Martinelli, A. *Soft Matter* **2014**, *10*, 5618−5627.
(22) Iacob, C.; Sangoro, J. R.; Papadopoulos, P.; Schubert, T.; Naumov, S.; Valiullin, R.; Karger, J.; Kremer, F. *Phys. Chem. Chem. Phys.* **2010**, *12*, 13798−13803.
(23) Han, K. S.; Wang, X.; Dai, S.; Hagaman, E. W. *J. Phys. Chem. C* **2013**, *117*, 15754−15762.
(24) Giammanco, C. H.; Kramer, P. L.; Yamada, S. A.; Nishida, J.; Tamimi, A.; Fayer, M. D. *J. Phys. Chem. B* **2016**, *120*, 549−556.
(25) Giammanco, C. H.; Kramer, P. L.; Yamada, S. A.; Nishida, J.; Tamimi, A.; Fayer, M. D. *J. Chem. Phys.* **2016**, *144*, 104506.
(26) Giammanco, C. H.; Yamada, S. A.; Kramer, P. L.; Tamimi, A.; Fayer, M. D. *J. Phys. Chem. B* **2016**, *120*, 6698−6711.
(27) Tamimi, A.; Bailey, H. E.; Fayer, M. D. *J. Phys. Chem. B* **2016**, *120*, 7488−7501.
(28) Tamimi, A.; Fayer, M. D. *J. Phys. Chem. B* **2016**, *120*, 5842−5854.
(29) Shin, J. Y.; Yamada, S. A.; Fayer, M. D. *J. Am. Chem. Soc.* **2017**, *139*, 311−323.
(30) Fayer, M. D. *Physiology* **2011**, *26*, 381−392.
(31) Fayer, M. D.; Levinger, N. E. *Annu. Rev. Anal. Chem.* **2010**, *3*, 89−107.
(32) Edward, J. T. *J. Chem. Educ.* **1970**, *47*, 261.
(33) Ciancaleoni, G.; Zuccaccia, C.; Zuccaccia, D.; Macchioni, A. NMR Techniques for Investigating the Supramolecular Structure of Coordination Compounds in Solution. In *Techniques in Inorganic Chemistry*; CRC Press: 2010; pp 129−180.
(34) Maiella, P. G.; Schoppelrei, J. W.; Brill, T. B. *Appl. Spectrosc.* **1999**, *53*, 351−355.
(35) Kumar, S. K.; Tamimi, A.; Fayer, M. *J. Chem. Phys.* **2012**, *137*, 184201.
(36) Nishida, J.; Tamimi, A.; Fei, H.; Pullen, S.; Ott, S.; Cohen, S. M.; Fayer, M. D. *Proc. Natl. Acad. Sci. U. S. A.* **2014**, *111*, 18442−18447.
(37) Tokmakoff, A. *J. Chem. Phys.* **1996**, *105*, 1−12.
(38) Kwak, K.; Park, S.; Finkelstein, I. J.; Fayer, M. D. *J. Chem. Phys.* **2007**, *127*, 124503.
(39) Kwak, K.; Rosenfeld, D. E.; Fayer, M. D. *J. Chem. Phys.* **2008**, *128*, 204505.
(40) Kai, T.; Duan, S. CO_2 Capture by Membrane. In *Handbook of Climate Change Mitigation and Adaptation*; Chen, W.-Y., Suzuki, T., Lackner, M., Eds.; Springer: New York, NY, 2014; pp 1−28.
(41) Kenkre, V.; Tokmakoff, A.; Fayer, M. *J. Chem. Phys.* **1994**, *101*, 10618−10629.
(42) Owrutsky, J.; Raftery, D.; Hochstrasser, R. *Annu. Rev. Phys. Chem.* **1994**, *45*, 519−555.
(43) Moilanen, D. E.; Fenn, E. E.; Lin, Y.-S.; Skinner, J.; Bagchi, B.; Fayer, M. D. *Proc. Natl. Acad. Sci. U. S. A.* **2008**, *105*, 5295−5300.
(44) Lipari, G.; Szabo, A. *Biophys. J.* **1980**, *30*, 489−506.
(45) Wang, C.; Pecora, R. *J. Chem. Phys.* **1980**, *72*, 5333−5340.
(46) Kinosita, K., Jr; Ikegami, A.; Kawato, S. *Biophys. J.* **1982**, *37*, 461−464.
(47) Lipari, G.; Szabo, A. *J. Am. Chem. Soc.* **1982**, *104*, 4546−4559.
(48) Kramer, P. L.; Giammanco, C. H.; Fayer, M. D. *J. Chem. Phys.* **2015**, *142*, 212408.
(49) Tan, H.-S.; Piletic, I. R.; Fayer, M. D. *J. Chem. Phys.* **2005**, *122*, 174501.
(50) Richert, R. *Annu. Rev. Phys. Chem.* **2011**, *62*, 65−84.
(51) Thompson, W. H. *Annu. Rev. Phys. Chem.* **2011**, *62*, 599−619.
(52) Krutyeva, M.; Wischnewski, A.; Monkenbusch, M.; Willner, L.; Maiz, J.; Mijangos, C.; Arbe, A.; Colmenero, J.; Radulescu, A.; Holderer, O. *Phys. Rev. Lett.* **2013**, *110*, 108303.
(53) Antelmi, D. A.; Kékicheff, P.; Richetti, P. *Langmuir* **1999**, *15*, 7774−7788.
(54) Mezger, M.; Schröder, H.; Reichert, H.; Schramm, S.; Okasinski, J. S.; Schöder, S.; Honkimäki, V.; Deutsch, M.; Ocko, B. M.; Ralston, J. *Science* **2008**, *322*, 424−428.
(55) Sieffert, N.; Wipff, G. *J. Phys. Chem. C* **2008**, *112*, 19590−19603.
(56) Bovio, S.; Podesta, A.; Lenardi, C.; Milani, P. *J. Phys. Chem. B* **2009**, *113*, 6600−6603.
(57) Mezger, M.; Schramm, S.; Schröder, H.; Reichert, H.; Deutsch, M.; De Souza, E. J.; Okasinski, J. S.; Ocko, B. M.; Honkimäki, V.; Dosch, H. *J. Chem. Phys.* **2009**, *131*, 094701.
(58) Shimizu, K.; Pensado, A.; Malfreyt, P.; Pádua, A. A.; Lopes, J. N. C. *Faraday Discuss.* **2012**, *154*, 155−169.
(59) Elbourne, A.; Voïtchovsky, K.; Warr, G. G.; Atkin, R. *Chem. Sci.* **2015**, *6*, 527−536.
(60) Parr, D.; Chrestenson, J.; Malik, K.; Molter, M.; Zibart, C.; Egan, B.; Haverhals, L. M. *ECS Trans.* **2015**, *66*, 35−42.
(61) Jurado, L. A.; Kim, H.; Arcifa, A.; Rossi, A.; Leal, C.; Spencer, N. D.; Espinosa-Marzal, R. M. *Phys. Chem. Chem. Phys.* **2015**, *17*, 13613−13624.
(62) Anaredy, R. S.; Shaw, S. K. *Langmuir* **2016**, *32*, 5147−5154.
(63) Amith, W. D.; Hettige, J. J.; Castner, E. W.; Margulis, C. J. *J. Phys. Chem. Lett.* **2016**, *7*, 3785−3790.
(64) Huang, X.; Margulis, C. J.; Li, Y.; Berne, B. J. *J. Am. Chem. Soc.* **2005**, *127*, 17842−17851.
(65) Cadena, C.; Anthony, J. L.; Shah, J. K.; Morrow, T. I.; Brennecke, J. F.; Maginn, E. J. *J. Am. Chem. Soc.* **2004**, *126*, 5300−5308.
(66) Hou, Y.; Baltus, R. E. *Ind. Eng. Chem. Res.* **2007**, *46*, 8166−8175.
(67) Kramer, P. L.; Nishida, J.; Giammanco, C. H.; Tamimi, A.; Fayer, M. D. *J. Chem. Phys.* **2015**, *142*, 184505.
(68) Kramer, P. L.; Nishida, J.; Fayer, M. D. *J. Chem. Phys.* **2015**, *143*, 124505.
(69) Wong, D. B.; Giammanco, C. H.; Fenn, E. E.; Fayer, M. D. *J. Phys. Chem. B* **2013**, *117*, 623−635.
(70) Fecko, C. J.; Eaves, J. D.; Loparo, J. J.; Tokmakoff, A.; Geissler, P. L. *Science* **2003**, *301*, 1698.
(71) Nishida, J.; Fayer, M. D. *J. Phys. Chem. C* **2017**, *121*, 11880−11890.
(72) Daly, C. A.; Berquist, E. J.; Brinzer, T.; Garrett-Roe, S.; Lambrecht, D. S.; Corcelli, S. A. *J. Phys. Chem. B* **2016**, *120*, 12633−12642.
(73) Gierer, V. A.; Wirtz, K. *Z. Naturforsch., A: Phys. Sci.* **1953**, *8*, 532.
(74) Perrin, F. *J. Phys. Radium* **1936**, *7*, 1−11.
(75) Moganty, S. S.; Baltus, R. E. *Ind. Eng. Chem. Res.* **2010**, *49*, 9370−9376.
(76) Moya, C.; Palomar, J.; Gonzalez-Miquel, M.; Bedia, J.; Rodriguez, F. *Ind. Eng. Chem. Res.* **2014**, *53*, 13782−13789.
(77) Scovazzo, P.; Kieft, J.; Finan, D. A.; Koval, C.; DuBois, D.; Noble, R. *J. Membr. Sci.* **2004**, *238*, 57−63.
(78) Budhathoki, S.; Shah, J. K.; Maginn, E. J. *Ind. Eng. Chem. Res.* **2017**, *56*, 6775−6784.

DOI: 10.1021/jacs.7b05759
J. Am. Chem. Soc. 2017, 139, 11222−11232